arXiv:2505.13795v2 [cond-mat.mtrl-sci] 30 May 2025

SUBSTRATE EFFECT ON ELECTRONIC BAND STRUCTURE AND TOPOLOGICAL PROPERTY IN MONOLAYER V_2O_3 MAGNETIC TOPOLOGICAL INSULATOR

Zheng Wang[1,#], **Jingshen Yan**[1,#], **Shu-Shen Lyu**[1−3], **Kaixuan Chen**[1−3,*]
[1]School of Materials, Shenzhen Campus of Sun Yat-sen University, Shenzhen, 518107, PR China,
[2]Guangdong Engineering Technology Research Centre
for Advanced Thermal Control Material and System Integration (ATCMSI),
Sun Yat-sen University, Guangzhou, 510275, PR China,
[3]Huizhou Research Institute, Sun Yat-sen University, Huizhou, 516081, PR China.
#These authors contribute equally to this work.
E-mail: chenkx26@mail.sysu.edu.cn

September 18, 2025

ABSTRACT

Monolayer V_2O_3, a two-dimensional magnetic topological insulator with intrinsic ferromagnetic order and a nontrivial band gap, offers a promising platform for realizing quantum anomalous Hall (QAH) states. Using first-principles density functional theory calculations, we systematically investigate the impact of substrate selection on its electronic and topological properties. By modeling heterostructures with van der Waals (vdW) substrates, we demonstrate that non-magnetic substrates such as h-BN preserve the QAH phase with a Chern number C = 1, maintaining gapless chiral edge states. In contrast, ferromagnetic substrates induce extra electrons, destroying the topological order by shifting the Fermi level. These findings establish substrate engineering as a pivotal strategy for experimental realization of dissipationless edge transport in V_2O_3-based vdW heterostructures, advancing their potential applications as low-power topological electronics.

1 Introduction

Topological insulators (TIs), a novel class of quantum materials, have garnered significant attention because of their unique properties, which exhibit bulk insulating while simultaneously possessing conductive states on their surface (or edges)[22, 5, 6]. Among them, as recently predicted theoretically, two-dimensional (2D) honeycomb lattice V_2O_3 was proposed as a candidate for a 2D magnetic topological insulator, emerging potential to host quantum anomalous Hall (QAH) states due to its experimental feasibility, intrinsic ferromagnetism, and robust band gap[18, 21].

However, the 2D materials must be supported on substrates, whose interaction with the film can significantly modify its electronic and topological features[23, 26, 28]. In particular, substrate-induced symmetry breaking or magnetic proximity effects may jeopardize the QAH phase[11, 4].

For d-orbital-mediated magnetic topological insulators, the circumstantial issue of substrate selection, which influences or disrupts the topological character of V_2O_3, still remains elusive. In this work, we systematically investigate the impact of both magnetic and non-magnetic substrates on the electronic structure and topological properties of V_2O_3 film using first-principles calculations. We show that while non-magnetic insulator substrates preserve the QAH state, ferromagnetic substrates disrupt the topological order due to the extra magnetic moments induced metallic state of system. Our findings demonstrate the crucial role of substrate selection in realizing and controlling topological phases in 2D magnetic TIs.

2 Results and discussion

To investigate the influence of substrates on the topological properties of V_2O_3 thin films (the electronic properties are shown in Fig.1), we selected several 2D materials exhibiting good lattice matching with V_2O_3 to construct simplified heterostructures. The spin-orbit coupling (SOC)-induced band splitting of the V_2O_3 film was labeled as the topological index.

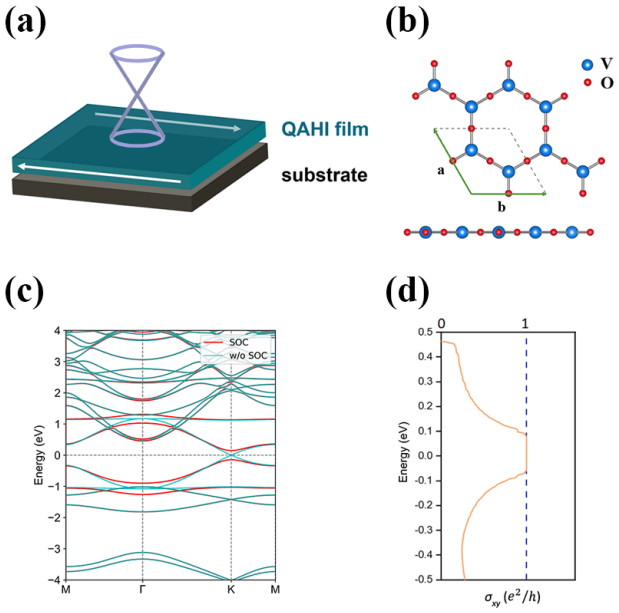

Figure 1: (a) Schematic demonstration of heterostructure, i.e., V_2O_3 supported on substrates. (b) Atomistic structure of monolayer V_2O_3 (top view and side view). (c) Electronic band structure of monolayer V_2O_3 with and without SOC effect. (d) The corresponding quantized QAH conductance.

Table 1: Structural information of the constructed V_2O_3-substrates heterostructures.

Substrates	Space Group	Lattice constant (Å)	Band Gap (eV)	Stacking configuration (V_2O_3/substrates)	Interlayer spacing (Å)	Lattice Mismatch (%)	Heterostructures parameters (Å)
$CoCl_2$[2]	$P\bar{3}m1$	3.54	0.08	$1\times1/\sqrt{3}\times\sqrt{3}$	2.8	0.5	a=b=6.18
$FeCl_2$[20]	$P\bar{3}m1$	3.57	0	$1\times1/\sqrt{3}\times\sqrt{3}$	3.2	0.1	a=b=6.18
$NiCl_2$[9]	$P\bar{3}m1$	3.48	0	$1\times1/\sqrt{3}\times\sqrt{3}$	3.4	2.6	a=b=6.18
$MgCl_2$[13]	$P\bar{3}m1$	3.64	5.90	$1\times1/\sqrt{3}\times\sqrt{3}$	3.2	2.0	a=b=6.19
$CrCl_3$[3]	$R\bar{3}$	6.00	1.52	1×1/1×1	2.9	2.9	a=b=6.14
WTe_2[10]	$P6_3mmc$	3.56	0.94	$1\times1/\sqrt{3}\times\sqrt{3}$	3.3	0.2	a=b=6.13
h-BN[17]	$R\bar{3}$	2.50	4.90	2×2/5×5	3.5	1.1	a=b=12.51

The corresponding substrates are listed in Table1, wherein MCl_2 (M=Fe, Co, Ni), $CrCl_3$ are d-orbital-mediated magnetic materials, while $MgCl_2$, h-BN, and WTe_2 are non-magnetic insulator materials. The heterostructures were constructed by directly stacking the V_2O_3 film onto the selected substrates along the z-axis, ensuring a lattice mismatch of less than 5% for all systems.

Given the prevalent use of magnetic substrates to drive topological insulator phase transitions[12], we initially investigated whether the magnetic proximity effect induced by van der Waals layers would influence the topological properties of V_2O_3. Co(Fe,Ni)Cl_2 monolayers are employed as substrates since they have high lattice matching and were synthesised experimentally before[2, 20, 9]. The optimized heterostructures are shown in Fig.2(a, b, c) presenting the side/top view and supercell, respectively. The V atoms in the upper layer align directly with the lower M (Fe,Co,Ni,Mg) atoms along the z-axis. The crystal structure exhibits a van der Waals layered framework, with no obvious lattice distortion observed from the supercell perspective. Furthermore, we considered both AFM and FM coupling between the film and substrates to investigate its effect, as shown in Fig.2(d).

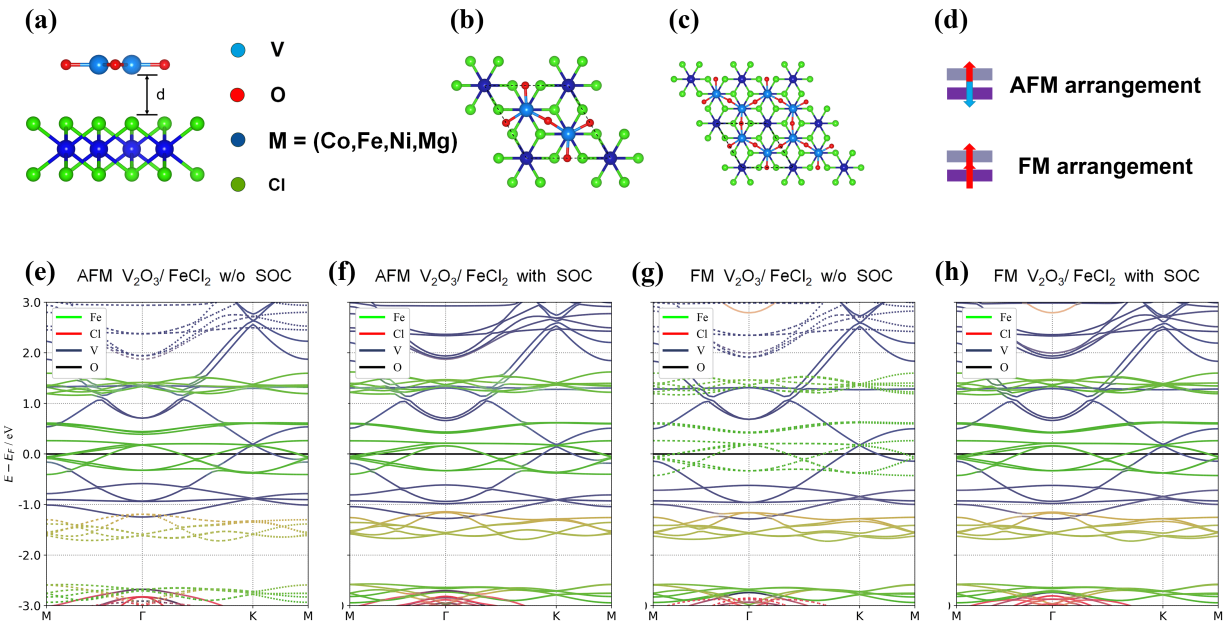

Figure 2: (a) top view, (b) side view, (c) supercell perspective of V_2O_3/MCl_2 heterostructures. (d) magnetic configurations of V_2O_3/MCl_2 heterostructures. (e) and (f) band structures of AFM $V_2O_3/FeCl_2$ with/without SOC. (g) and (h) band structures of FM $V_2O_3/FeCl_2$ with/without SOC.

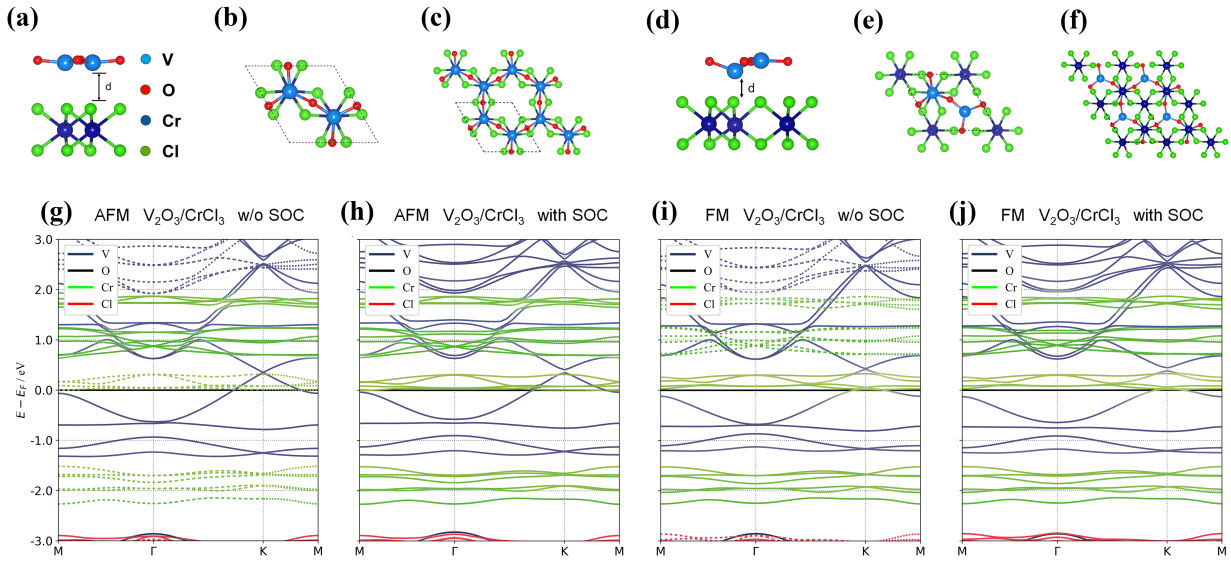

Figure 3: (a-c)/(d-f) side view, top view and supercell perspective of AA/AB stacking $V_2O_3/CrCl_3$ heterostructures. (g) and (h) band structures of AFM AA stacking $V_2O_3/CrCl_3$ with/without SOC. (g) and (h) band structures of FM AA stacking $V_2O_3/CrCl_3$ with/without SOC.

As reported in previous studies, the topological properties of V_2O_3 originate from a Dirac point (contributed by V d_{xz},d_{yz} orbitals) at the high symmetry $K(K')$-point, which arises due to a C_{3v} symmetry-protected band crossing, in combination with band inversion induced by the strong SOC effect of the d-orbital electrons[21]. Given the strong correlation between the electronic band structure and topological properties, we performed spin-polarized and SOC

calculations on V_2O_3/MCl_2 heterostructures. It should be noted that the MX_2 primitive cell has a lattice constant of approximately 3.5Å, when combining a 1×1 V_2O_3 unit cell with a 2×2 MX_2 cells resulting in a lattice mismatch exceeding 10%, which would introduce significant lattice distortion. Therefore, $\sqrt{3} \times \sqrt{3}$ MX_2 substrates were employed (see Fig.3a-c). In the AFM coupling system, as illustrated in Fig.2(e), the spin-up bands near the Fermi level orbitals are primarily contributed by V (blue line) and Fe (green line). At the K-point, the Dirac cone of the V bands overlaps with the Fe d orbitals. This hybridization occurs between orbitals of the same spin and energy, which can also be observed from the perspective of the wavefunction at the K point correspondingly in Fig.S1(a,b). The spin-up wave function of the Dirac cone slightly distributes on the lower $FeCl_2$ layer, dominated by the $d-d$ hybridization between V and Fe. When SOC is considered, the band structure (Fig.2(f)) and the corresponding wavefunctions exhibit negligible changes. The Dirac cone remains almost gapless under SOC, thereby destroying the topological nature of the V_2O_3 film. In the FM counterpart shown in Fig.2(g), the positions of the spin-up and spin-down $FeCl_2$ bands are reversed, thus the bands hybridization at K-point in AFM are decoupled by flipped magnetic moments. Moreover, the wavefunctions at the band crossing are not contributed by the Fe d orbitals. When SOC is included (Fig.2(h)), a tiny SOC splitting appears at the Dirac cone of V_2O_3, as same as the AFM configuration. The SOC splitting energies are listed in Table2, we find the magnetic coupling configuration appears to have no significant influence on the SOC induced splitting energy.

Table 2: Calculated SOC splitting energy (in meV) of V_2O_3 supported on different substrates under AFM/FM magnetic configuration.

Substrates	$CoCl_2$		$FeCl_2$		$NiCl_2$	
Magnetic Configuration	AFM	FM	AFM	FM	AFM	FM
Splitting energy	35	38	40	38	42	37

Besides, magnetic substrates introduce magnetic moments arising from extra unpaired electrons, effectively resulting in an electron-doped system. This doping shifts the Fermi level, thereby destroying the topological nature of the system. But it is still necessary to investigate the mechanism of broken topology, whether correlated with other magnetic substrates or not. We further employ 2D magnetic insulator $CrCl_3$, which possesses $R\bar{3}$ point group allowing different heterostructure stacking configurations with V_2O_3 film, AA and AB[14]. Fig.3(a-f) present the top view, side view, supercell view of AA and AB stacking system. The AA stacking heterostructure is shown in Fig.3(a-c), the upper V atoms are directly align with the lower Cr atoms, remaining 2.9Å layer distance; the hexagonal structure of V_2O_3 highly overlaps with the hexagonal structure of lower $CrCl_3$ layer (Fig.3(c)). While for the AB stacking system, half of the V atoms are positioned above the vacancy site in the lower $CrCl_3$ layer. The optimized lattice exhibits severe lattice distortion along z-axis, so we excluded it from further analysis. Analogous to the band structures of V_2O_3/MCl_2 discussed above, the Fermi level near the two magnetic configurations(AFM and FM) is mainly occupied by V and Cr, as shown in Fig.3(g,i). In FM system, the $d-d$ orbital overlapping induces significant hybridization, rendering discontinuous splitting of the V bands near the band crossing. When SOC is considered, as presented in Fig.3(h,j), the SOC induced splitting energy of 63 meV occurs in both configurations at the band crossing. The corresponding wavefunctions in real space are posted in Fig.S1(c,d). It should be noted that the magnetic coupling configuration does not significantly influence the SOC-induced band splitting in V_2O_3. The observed differences in SOC splitting energy between V_2O_3/MCl_2 and $V_2O_3/CrCl_3$ appear to be primarily governed by the degree of band overlap or the density of states at the overlapping regions, which are shown in Fig.S4.

Subsequently, we investigate the effect of interlayer spacing on the SOC-induced band splitting in V_2O_3 thin films by explicitly varying the interlayer distance within the heterostructures. Notably, an excessively small interlayer spacing can induce strong bonding between V_2O_3 and $CrCl_3$ under AFM coupling; we then focus solely on the FM coupling. As listed in Table3, the splitting energy increases with increasing interlayer spacing, exhibiting a clear correlation between these two parameters. When the interlayer spacing is set to 2.5 Å, the band structure of V_2O_3 film is significantly altered by strong orbital hybridization, the band crossing disappears. The corresponding electronic structures and wave functions are shown in Fig.S3.

Table 3: Calculated SOC splitting energy (in meV) of V_2O_3 supported on $CrCl_3$ substrate under FM coupling with different interlayer distance.

Interlayer spacing (Å)	2.5	3.0	3.5	4.0	4.5
Splitting energy (meV)	N/A	66	76	80	83

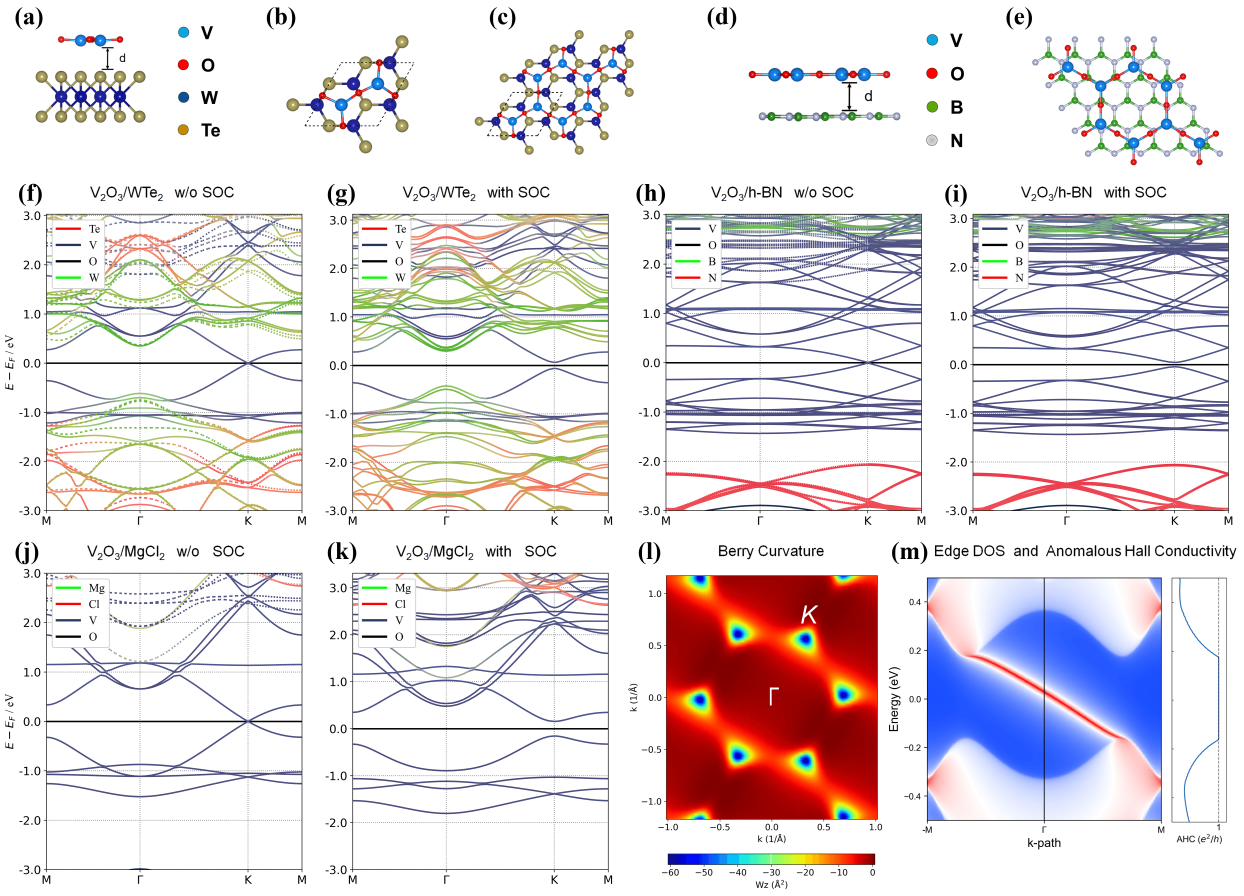

Figure 4: (a-c) side view, top view and supercell perspective of V_2O_3/WTe_2 heterostructure. (d,e) side view and top view of V_2O_3/h-BN heterostructure. (f) and (g) band structures of V_2O_3/WTe_2 with/without SOC. (h) and (i) band structures of V_2O_3/h-BN with/without SOC. (j) and (k) band structures of $V_2O_3/MgCl_2$ with/without SOC. (l) and (m) non-zero berry curvature, chiral edge state and corresponding anomalous Hall conductivity of $V_2O_3/MgCl_2$.

Regarding non-magnetic substrates, we selected monolayer h-BN, a widely used experimental substrate; along with non-magnetic $MgCl_2$ and WTe_2, a material with strong SOC driven by heavy elements and broken inversion symmetry[17, 27, 13]. The optimized lattice structure of the V_2O_3/WTe_2 heterostructure is shown in Fig. 4(a,b). Differently from the previously discussed MCl_2 systems, each V atom in this system is aligned directly above a hollow site of the lower WTe_2 hexagon. Fig. 4(c) presents a supercell view of the heterostructure, where the reshaped lattice constant slightly decreases to 6.13 Å, introducing a small twist in the V_2O_3 film. The corresponding band structures are shown in Fig.4(f,g), the strong $d-d$ orbital hybridization occurs away from the Fermi level; due to the non-magnetic substrate, the parts of V_2O_3 bands basically retain the characteristics as a single layer, maintaining the linear Dirac cone at the K-point. Besides, the WTe_2 is introduced a spin polarization splitting, reaching up to 70 meV. When considering SOC effect, as shown in Fig.4(g), the Dirac cone originating from the V_2O_3 layer opens a band gap of approximately 120 meV. Additionally, the bands contributed by the WTe_2 substrate exhibit significant SOC splitting near the high-symmetry Γ and M points, reflecting the intrinsic strong SOC of WTe_2. However, this substrate-induced SOC effect does not constructively interact with the on-site SOC of the V_2O_3.

Fig. 4(d,e) show the side and top views of the V_2O_3/h-BN heterostructure, The V_2O_3 structure exhibits no significant change when deposited on the h-BN substrate. The corresponding band structure are shown in Fig. 4(h,i), the band crossing of V_2O_3 is also located at the Fermi level, and is introduced 89meV band gap by SOC effect. The optimized structure of the $V_2O_3/MgCl_2$ heterostructure is shown in Fig.2(a), and the corresponding band structures are presented in Fig.4(j,k). Due to the electronic configuration of Mg (outermost $3s^2$ electrons), there is only minor orbital overlap between the Mg s orbitals and Cl p orbitals near the V_2O_3 bands. As shown in Fig.4(k), upon including SOC, the

$V_2O_3/MgCl_2$ heterostructure exhibits a remarkable SOC-induced band gap of approximately 310 meV, which is larger than that observed on other substrates.

To determine whether the SOC gap retains a topological nontrivial feature, we constructed a tight-binding (TB) model of the heterostructure based on Wannier90 and calculated the Berry curvature, edge states, and anomalous Hall conductivity. The results confirm that the opened SOC gap remains topologically nontrivial. As shown in Fig.4(l), a nonzero Berry curvature is concentrated near the K point in the Brillouin zone, contributing to the nontrivial topology. Fig.4(m) displays the chiral edge states crossing the Fermi level and the inset on the right side shows the anomalous Hall conductivity, where a quantized conductivity plateau near the Fermi level indicates a Chern number of $C = 1$.

3 Conclusion

In summary, we have systematically studied the influence of substrate selection on the electronic structure and topological properties of monolayer V_2O_3 using first-principles calculations. Our results reveal that the topological band gap of V_2O_3 is directly correlated with the magnitude of orbital overlapping and interlayer spacing; non-magnetic substrates preserve the QAH phase with a Chern number of $C = 1$, while ferromagnetic substrates disrupt the TI feature via extra magnetic moments shifting Fermi level. These findings underscore the critical role of substrate engineering in stabilizing and tuning topological phases in two-dimensional magnetic materials.

References

[1] P. E. Blöchl. Projector augmented-wave method. *Physical Review B*, 50(24):17953–17979, December 1994. ISSN 0163-1829, 1095-3795.

[2] Antia S Botana and Michael R Norman. Electronic structure and magnetism of transition metal dihalides: Bulk to monolayer. *Physical Review Materials*, 3(4):044001, 2019.

[3] Xinghan Cai, Tiancheng Song, Nathan P Wilson, Genevieve Clark, Minhao He, Xiaoou Zhang, Takashi Taniguchi, Kenji Watanabe, Wang Yao, Di Xiao, et al. Atomically thin crcl3: an in-plane layered antiferromagnetic insulator. *Nano letters*, 19(6):3993–3998, 2019.

[4] C Cardoso, AT Costa, AH MacDonald, and J Fernández-Rossier. Strong magnetic proximity effect in van der waals heterostructures driven by direct hybridization. *Physical Review B*, 108(18):184423, 2023.

[5] Cui-Zu Chang, Chao-Xing Liu, and Allan H. MacDonald. Colloquium: Quantum anomalous hall effect. *Reviews of Modern Physics*, 95(1):011002, January 2023.

[6] M Michael Denner, Anastasiia Skurativska, Frank Schindler, Mark H Fischer, Ronny Thomale, Tomáš Bzdušek, and Titus Neupert. Exceptional topological insulators. *Nature communications*, 12(1):5681, 2021.

[7] Stefan Grimme, Jens Antony, Stephan Ehrlich, and Helge Krieg. A consistent and accurate ab initio parametrization of density functional dispersion correction (dft-d) for the 94 elements h-pu. *The Journal of Chemical Physics*, 132 (15):154104, 04 2010.

[8] G. Kresse and J. Furthmüller. Efficient iterative schemes for *ab initio* total-energy calculations using a plane-wave basis set. *Physical Review B*, 54(16):11169–11186, October 1996. ISSN 0163-1829, 1095-3795.

[9] Vadym V. Kulish and Wei Huang. Single-layer metal halides mx $_2$ (x = cl, br, i): Stability and tunable magnetism from first principles and monte carlo simulations. *Journal of Materials Chemistry C*, 5(34):8734–8741, 2017. ISSN 2050-7526, 2050-7534.

[10] Shuang Li, Feng-cai Lei, Xu Peng, Ruo-qi Wang, Jun-feng Xie, Ya-pan Wu, and Dong-sheng Li. Synthesis of semiconducting 2h-phase wte2 nanosheets with large positive magnetoresistance. *Inorganic Chemistry*, 59(17): 11935–11939, 2020.

[11] Chun-Liang Lin, Ryuichi Arafune, Kazuaki Kawahara, Mao Kanno, Noriyuki Tsukahara, Emi Minamitani, Yousoo Kim, Maki Kawai, and Noriaki Takagi. Substrate-induced symmetry breaking in silicene. *Physical review letters*, 110(7):076801, 2013.

[12] Jieyi Liu and Thorsten Hesjedal. Magnetic topological insulator heterostructures: A review. *Advanced Materials*, 35(27):2102427, 2023. ISSN 1521-4095.

[13] HR Mahida, Abhishek Patel, Deobrat Singh, Yogesh Sonvane, PB Thakor, and Rajeev Ahuja. First-principles calculations to investigate electronic structure and optical properties of 2d mgcl2 monolayer. *Superlattices and Microstructures*, 162:107132, 2022.

[14] Bruno Morosin and Albert Narath. X-ray diffraction and nuclear quadrupole resonance studies of chromium trichloride. *The Journal of Chemical Physics*, 40(7):1958–1967, 1964.

[15] Arash A. Mostofi, Jonathan R. Yates, Giovanni Pizzi, Young-Su Lee, Ivo Souza, David Vanderbilt, and Nicola Marzari. An updated version of wannier90: A tool for obtaining maximally-localised wannier functions. *Computer Physics Communications*, 185(8):2309–2310, 2014.

[16] John P. Perdew, Kieron Burke, and Matthias Ernzerhof. Generalized gradient approximation made simple. *Physical Review Letters*, 77(18):3865–3868, October 1996.

[17] Akshay M Satawara, Gaushiya A Shaikh, Sanjeev K Gupta, and PN Gajjar. Structural, electronic and optical properties of hexagonal boron-nitride (h-bn) monolayer: An ab-initio study. *Materials Today: Proceedings*, 47: 529–532, 2021.

[18] S. Surnev, L. Vitali, M. G. Ramsey, F. P. Netzer, G. Kresse, and J. Hafner. Growth and structure of ultrathin vanadium oxide layers on pd(111). *Physical Review B*, 61(20):13945–13954, May 2000. ISSN 0163-1829, 1095-3795.

[19] David J Thouless, Mahito Kohmoto, M Peter Nightingale, and Marcel den Nijs. Quantized hall conductance in a two-dimensional periodic potential. *Physical review letters*, 49(6):405, 1982.

[20] E. Torun, H. Sahin, S. K. Singh, and F. M. Peeters. Stable half-metallic monolayers of fecl2. *Applied Physics Letters*, 106(19):192404, 05 2015. ISSN 0003-6951. doi: 10.1063/1.4921096. URL `https://doi.org/10.1063/1.4921096`.

[21] H. P. Wang and Wei Luo. Prediction of high-temperature quantum anomalous hall effect in two-dimensional transition-metal oxides. *Physical Review B*, 95(12):125430, March 2017. ISSN 2469-9950, 2469-9969.

[22] Pinyuan Wang, Jun Ge, Jiaheng Li, Yanzhao Liu, Yong Xu, and Jian Wang. Intrinsic magnetic topological insulators. *The Innovation*, 2(2):100098, 2021. ISSN 2666-6758. doi: https://doi.org/10.1016/j.xinn.2021.100098. URL `https://www.sciencedirect.com/science/article/pii/S2666675821000230`.

[23] Zheng Wang, Jingshen Yan, Kaixuan Chen, and Shu-Shen Lyu. Effects of stacking configuration on the electronic and topological properties of v 2 o 3 bilayers. *Physical Review B*, 111(8):085425, 2025.

[24] QuanSheng Wu, ShengNan Zhang, Hai-Feng Song, Matthias Troyer, and Alexey A. Soluyanov. Wanniertools: An open-source software package for novel topological materials. *Computer Physics Communications*, 224:405–416, 2018.

[25] Feng Xue, Yusheng Hou, Zhe Wang, and Ruqian Wu. Two-dimensional ferromagnetic van der waals crc l 3 monolayer with enhanced anisotropy and curie temperature. *Physical review b*, 100(22):224429, 2019.

[26] Jingshen Yan, Kaixuan Chen, and Shu-Shen Lyu. Exchange coupling-induced giant spin splitting in two-dimensional m2x3/tmd heterostructures. *The Journal of Physical Chemistry C*, 128(46):19856–19865, 2024.

[27] AA Yanaki and VA Obolonchik. Preparation of transition-metal tellurides by means of hydrogen telluride. *Inorg. Mater*, 9:1855–1858, 1973.

[28] Jun-Tao Yang, Chao Jing, Yong-Chen Xiong, and Shi-Jun Luo. Electronic structures and magnetic properties of two-dimensional honeycomb-kagome structured v 2 o 3 monolayer and v 2 o 3 /m(0001) (m=zr and hf) system. *Journal of Magnetism and Magnetic Materials*, 564:170161, December 2022. ISSN 03048853.

[29] Yugui Yao, Leonard Kleinman, AH MacDonald, Jairo Sinova, T Jungwirth, Ding-sheng Wang, <? format?> Enge Wang, and Qian Niu. First principles calculation of anomalous hall conductivity in ferromagnetic bcc fe. *Physical review letters*, 92(3):037204, 2004.

SUPPLEMENTARY INFORMATION: SUBSTRATE EFFECT ON ELECTRONIC BAND STRUCTURE AND TOPOLOGICAL PROPERTY IN MONOLAYER V_2O_3 MAGNETIC TOPOLOGICAL INSULATOR

Zheng Wang[1,#], **Jingshen Yan**[1,#], **Shu-Shen Lyu**[1−3], **Kaixuan Chen**[1−3,*]
[1]School of Materials, Shenzhen Campus of Sun Yat-sen University, Shenzhen, 518107, PR China,
[2]Guangdong Engineering Technology Research Centre
for Advanced Thermal Control Material and System Integration (ATCMSI),
Sun Yat-sen University, Guangzhou, 510275, PR China,
[3]Huizhou Research Institute, Sun Yat-sen University, Huizhou, 516081, PR China.
#These authors contribute equally to this work.
E-mail: chenkx26@mail.sysu.edu.cn

September 18, 2025

1 Computational details

First-principles calculations were performed using density functional theory (DFT) as implemented in the Vienna Ab initio Simulation Package (VASP)[3]. The interactions between electrons and ions were treated using the projector augmented wave (PAW) method[1]. The exchange-correlation potential was described using the generalized gradient approximation (GGA) in the Perdew-Burke-Ernzerhof (PBE) form[5]. A plane-wave basis set with a kinetic energy cutoff of 500 eV was employed, and the Brillouin zone was sampled using an 11 × 11 × 1 Gamma-centered k-mesh. Self-consistent calculations were considered converged when the total energy difference was less than 10^{-6} eV, while atomic structures were optimized until the residual Hellmann-Feynman forces were below 0.01 eV/Å. To avoid spurious interactions due to periodic boundary conditions, a vacuum layer of 15 Å was added along the z-axis. The DFT+U approach was used to account for the on-site Coulomb interactions in the localized d orbitals, with Hubbard U parameters of 3.2 eV for vanadium only[]. Furthermore, vdW interactions were corrected using the DFT-D3 method proposed by Grimme[2].

The topological characteristic is confirmed by SOC-induced band splitting, berry curvature, edge state and AHC. All topology related calculations are based on Maximally Localized Wannier Functions (MLWFs) methods, as implemented in the Wannier90 and WannierTools packages[4, 7]. The Chern number is calculated by integrating Berry curvature over the first Brillouin Zone:

$$C = \frac{1}{2\pi} \sum_n \int_{\mathrm{BZ}} d^2k \Omega_n \tag{1}$$

Where $\Omega(k)$ is the Berry curvature which is calculated by Kubo formula[6, 8]:

$$\Omega_n(k) = -\sum_{n' \neq n} \frac{2\mathrm{Im} \langle \psi_{nk} | \upsilon_x | \psi_{n'k} \rangle \langle \psi_{n'k} | \upsilon_y | \psi_{nk} \rangle}{(\varepsilon_{n'} - \epsilon_n)^2} \tag{2}$$

2 Complement to figures

Wavefuctions at K point in real space of V_2O_3/MCl_2 heterostructures (M=Co,Ni).

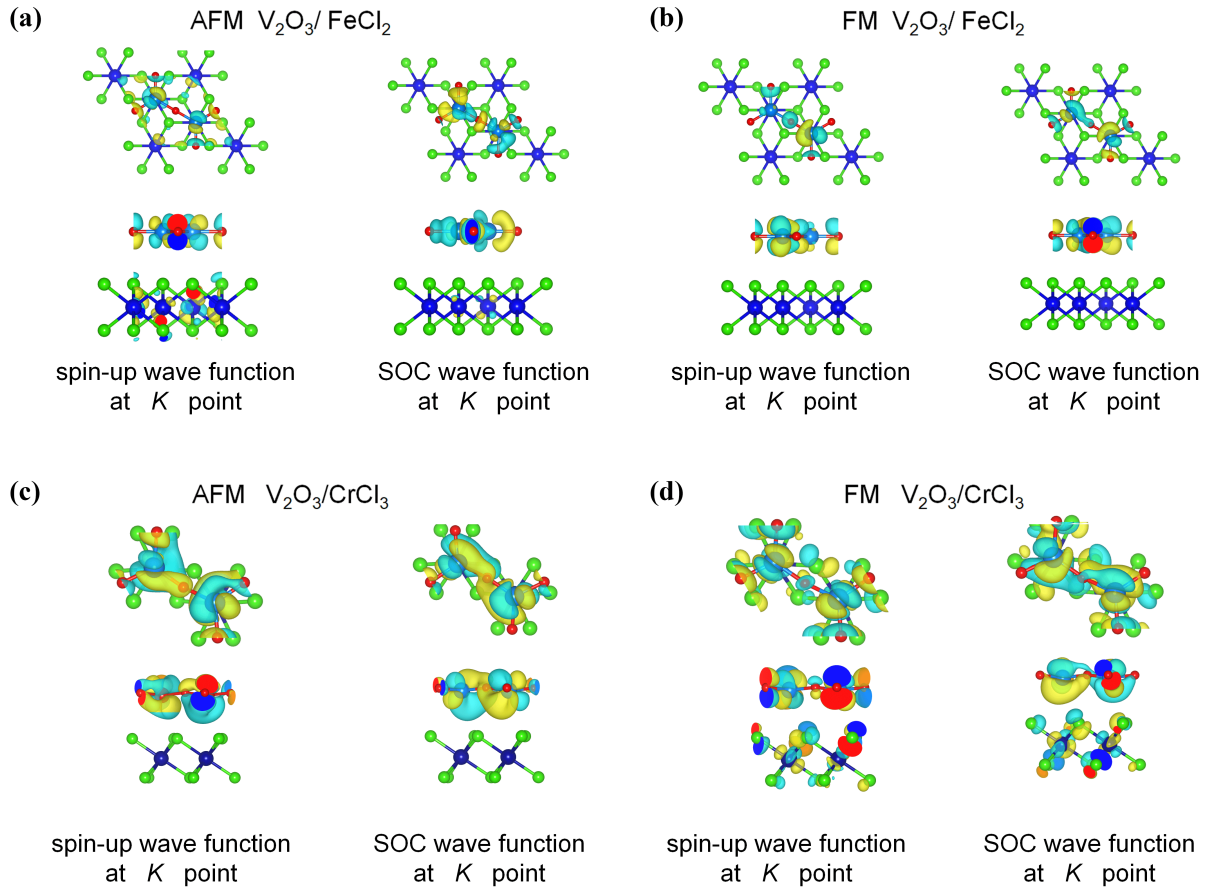

Figure 1: (a)/(b) spin-up/SOC wavefunction of V_2O_3/MCl_2 heterostructure under AFM coupling. (c)/(d) spin-up/SOC wavefunction of V_2O_3/MCl_2 heterostructure under FM coupling.

Band structure of V_2O_3/MCl_2 heterostructures (M=Co,Ni).

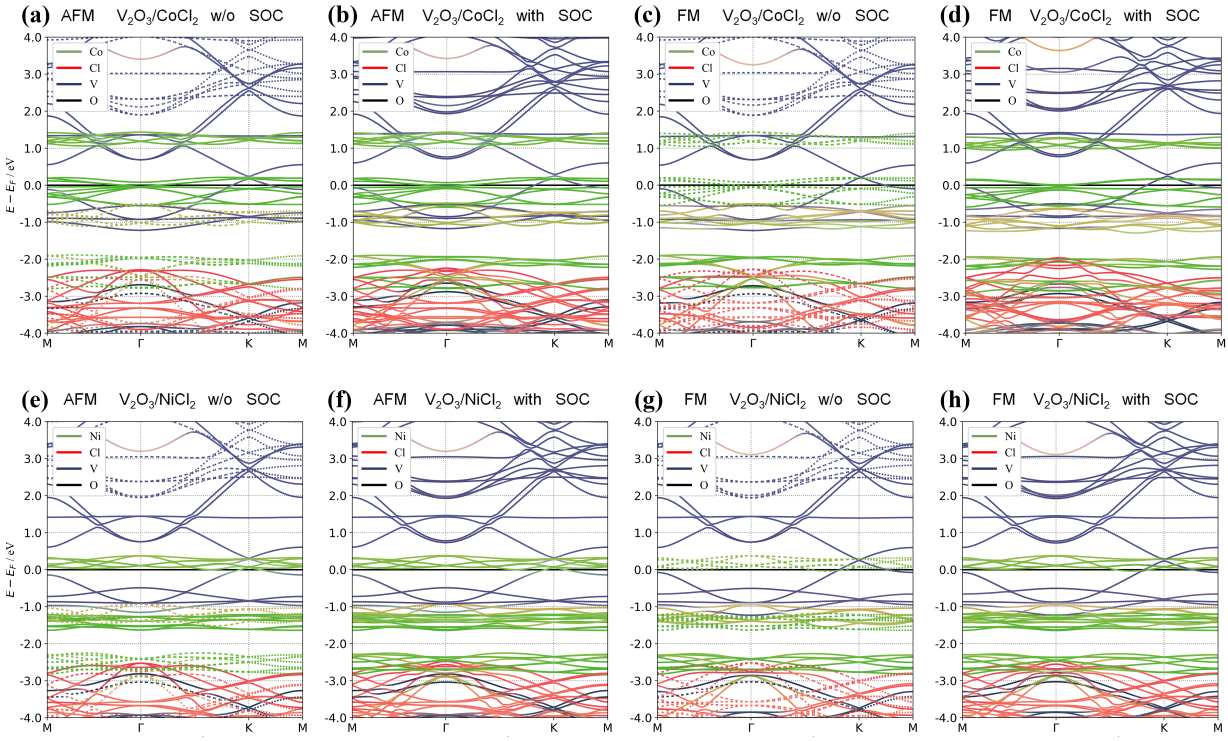

Figure 2: (a) and (b) band structures of AFM $V_2O_3/CoCl_2$ with/without SOC. (c) and (d) band structures of FM $V_2O_3/COCl_2$ with/without SOC. (e) and (f) band structures of AFM $V_2O_3/NiCl_2$ with/without SOC. (g) and (h) band structures of FM $V_2O_3/NiCl_2$ with/without SOC.

Band structures of AA stacking $V_2O_3/CrCl_3$ heterostructures with different interlayer spacings under AFM coupling.

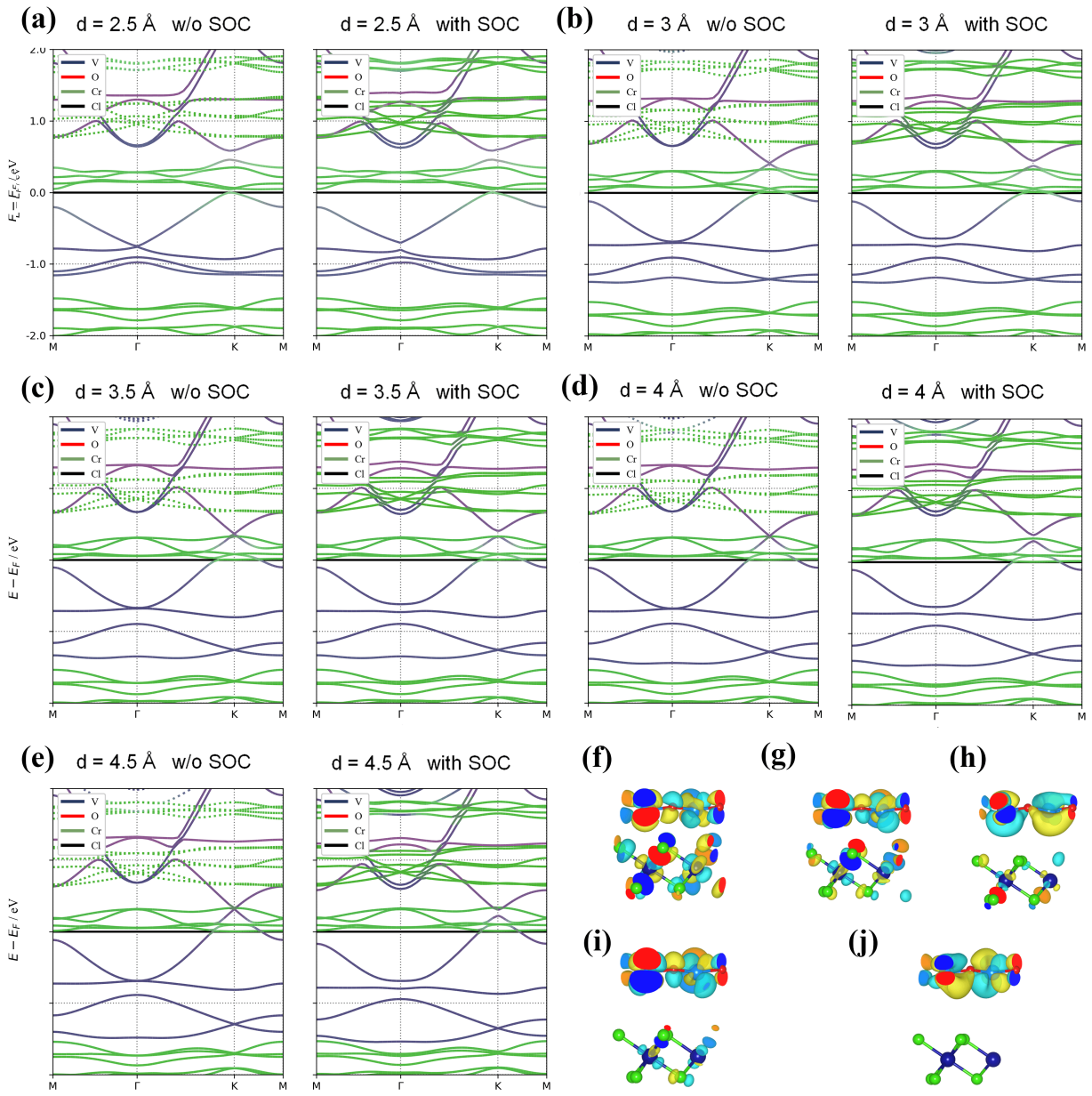

Figure 3: (a-e)spin polarization and SOC band diagram with interlayer spacing of 2.5 Å -4.5 Å. (f-j) real space wavefunctions distribution of band crossing points at K point corresponding to interlayer spacing of 2.5 Å -4.5 Å.

Density of states for all heterostructures.

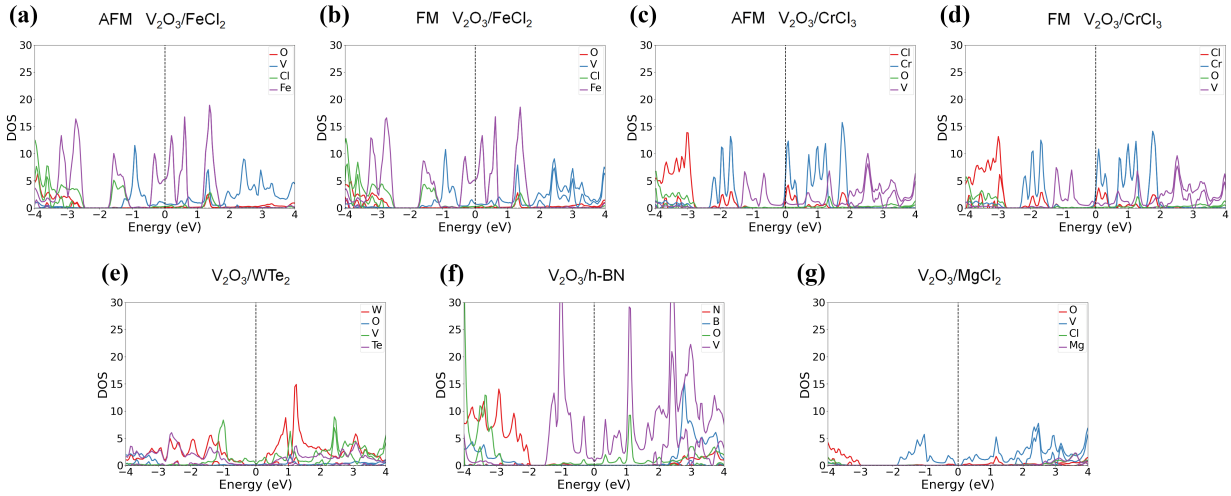

Figure 4: (a) $V_2O_3/FeCl_2$ under AFM coupling. (b) $V_2O_3/FeCl_2$ under FM coupling. (c) $V_2O_3/CrCl_3$ under AFM coupling. (d) $V_2O_3/CrCl_3$ under FM coupling. (e) V_2O_3/WTe_2. (f) V_2O_3/h-BN. (g) $V_2O_3/FeCl_2$

References

[1] P. E. Blöchl. Projector augmented-wave method. *Physical Review B*, 50(24):17953–17979, December 1994. ISSN 0163-1829, 1095-3795.

[2] Stefan Grimme, Jens Antony, Stephan Ehrlich, and Helge Krieg. A consistent and accurate ab initio parametrization of density functional dispersion correction (dft-d) for the 94 elements h-pu. *The Journal of Chemical Physics*, 132 (15):154104, 04 2010.

[3] G. Kresse and J. Furthmüller. Efficient iterative schemes for *ab initio* total-energy calculations using a plane-wave basis set. *Physical Review B*, 54(16):11169–11186, October 1996. ISSN 0163-1829, 1095-3795.

[4] Arash A. Mostofi, Jonathan R. Yates, Giovanni Pizzi, Young-Su Lee, Ivo Souza, David Vanderbilt, and Nicola Marzari. An updated version of wannier90: A tool for obtaining maximally-localised wannier functions. *Computer Physics Communications*, 185(8):2309–2310, 2014.

[5] John P. Perdew, Kieron Burke, and Matthias Ernzerhof. Generalized gradient approximation made simple. *Physical Review Letters*, 77(18):3865–3868, October 1996.

[6] David J Thouless, Mahito Kohmoto, M Peter Nightingale, and Marcel den Nijs. Quantized hall conductance in a two-dimensional periodic potential. *Physical review letters*, 49(6):405, 1982.

[7] QuanSheng Wu, ShengNan Zhang, Hai-Feng Song, Matthias Troyer, and Alexey A. Soluyanov. Wanniertools: An open-source software package for novel topological materials. *Computer Physics Communications*, 224:405–416, 2018.

[8] Yugui Yao, Leonard Kleinman, AH MacDonald, Jairo Sinova, T Jungwirth, Ding-sheng Wang, <? format?> Enge Wang, and Qian Niu. First principles calculation of anomalous hall conductivity in ferromagnetic bcc fe. *Physical review letters*, 92(3):037204, 2004.